Proton-proton bremsstrahlung below and above pion threshold: Influence of the Δ isobar

F. de Jong,[1,2,3] K. Nakayama,[1,2] and T.-S. H. Lee[4]
[1]*Department of Physics and Astronomy, University of Georgia, Athens, Georgia 30602*
[2]*Institut für Kernphysik, Forschungszentrum Jülich, 52428 Germany*
[3]*Kernfysisch Versneller Instituut, 9747 AA Groningen, The Netherlands*
[4]*Physics Division, Argonne National Laboratory, Argonne, Illinois 60439*
(Received 9 December 1994)

The proton-proton bremsstrahlung is investigated within a coupled-channel model with the Δ degree of freedom. The model is consistent with the NN scattering up to 1 GeV and the $\gamma N\Delta$ vertex determined in the study of pion photoproduction reaction. It is found that the Δ excitation can significantly improve the agreements with the $pp \to pp\gamma$ at $E_{\rm lab} = 280$ MeV. Predictions at $E_{\rm lab} = 550$ and 800 MeV are presented for future experimental tests.

PACS number(s): 13.75.Cs, 24.10.Eq, 25.40.Ve, 25.40.Ep

I. INTRODUCTION

The nucleon-nucleon bremsstrahlung ($NN\gamma$) reaction has long been considered as a tool to investigate the off-shell behavior of the NN interaction. With the availability of new experimental data of the $pp \to pp\gamma$ reaction [1, 2], theoretical interest has been revived recently [3–9]. As a start, it is sufficient to consider only the one-nucleon current to investigate this reaction since the leading interaction current due to one-pion exchange vanishes identically in the $pp\gamma$ reaction. In a calculation taking into account the relativistic features of the one-nucleon current [4, 5], the sensitivity of the $pp \to pp\gamma$ spin observables to the NN off-shell dynamics was demonstrated. Although the calculated analyzing powers are in general in good agreement with the data, the cross-section results are more controversial. In Ref. [1] a normalization factor of 2/3 was proposed to account for the major discrepancy with the data. However, this discrepancy might also indicate the importance of new mechanisms not included in the calculations, thus omitting the need of this rather arbitrary normalization factor. In Ref. [10], we have explored qualitatively the mechanisms due to the Δ degree of freedom. The main objective of this work is to present a consistent approach to quantify our investigation. This is accomplished by extending the coupled-channel formulation of NN scattering developed by Lee and Matsuyama [11, 12] to include the electromagnetic interactions introduced by de Jong *et al.* [10].

The effect of the Δ excitation on $NN\gamma$ has been investigated in the past using very crude models. Bohannon, Heller, and Thompson [13] derived the one-pion-exchange Δ current by taking the static nucleon limit of the pion photoproduction amplitude. The Δ width was neglected and hence their model is limited to low energies. They found that the Δ effect is negligibly small in the np bremsstrahlung. No calculation of the pp bremsstrahlung based on their Δ current has been reported. In contrast to the $np\gamma$ process, where the effect of the Δ isobar is greatly reduced by cancellations between the different diagrams involved due to isospin factors, the Δ effects may be significant in $pp\gamma$ reactions. Tiator *et al.* [14] evaluate the contributions of the radiative Δ decay in the Born approximation and add these incoherently to the nucleonic contributions which were calculated using the soft photon approximation (SPA). Although Szyjewicz and Kamal [15] evaluated all one-pion-exchange Δ contributions and add them coherently, their $pp\gamma$ calculation was carried out using only the Born approximation. In our previous work [10], we added the single-scattering Δ-decay diagrams coherently to a state of the art calculation of the nucleonic current contribution and found a significant effect. In the present paper we go beyond this in two respects. First, we use off-shell T-matrix elements that are generated from a meson-exchange coupled $NN \oplus N\Delta \oplus \pi NN$ model which is constrained by the NN scattering up to 1 GeV. The quality of the phase-shift fit of this T matrix is superior to the fit of the T matrix used in Ref. [10]. Second, we also include the rescattering diagrams induced by the presence of Δ degrees of freedom. We follow the approach of Ref. [4] to account for the relativistic features of the N and Δ currents. We will show that, even at energies below the pion threshold, the influence of the Δ on the $pp\gamma$ reaction is considerable and cannot be neglected in a quantitative comparison with the data.

In addition to giving a more complete description of $NN\gamma$ reaction at low energies, our approach is appropriate for making predictions in the intermediate energy region where the pion production through the Δ excitation becomes crucial. A good understanding of the $NN\gamma$ reaction at intermediate energies is needed to describe the production of hard photons in intermediate energy heavy-ion collisions [16, 17]. In these complicated processes the photon provides a clean probe of the reaction dynamics. Furthermore, recent studies of dilepton production in proton-nucleus collisions have shown that virtual NN bremsstrahlung and Δ decay are the dominant reaction mechanisms [18, 19]. The model presented in this paper can be used as the starting point of a mi-

croscopic approach to investigate both the photon and Δ productions in relativistic heavy-ion collisions.

In Sec. II, a coupled-channel formulation for $NN\gamma$ reaction will be presented. The results are presented in Sec. III. Section IV is devoted to discussions of future developments.

II. THE HAMILTONIAN MODEL OF NN AND $NN\gamma$ INTERACTIONS

To investigate the effect of the Δ on the $NN\gamma$ reaction, it is more transparent to employ a formulation including the Δ degree of freedom explicitly. In the first part of this section, we will describe such an approach based on an extension of the Hamiltonian model developed by Lee and Matsuyama [11, 12] to include the electromagnetic couplings introduced by de Jong *et al.* [10]. We then describe how the procedures introduced in Refs. [5, 10] are used to include the "minimum relativity" in the $NN\gamma$ calculation.

The objective of the formulation of Refs. [11, 12] was to obtain a consistent description of NN scattering from the low energy region ($E_{\rm lab} < 400$ MeV) to the intermediate energy region where the pion production through the Δ excitation becomes important. In contrast with the other πNN models [20], the formulation of Refs. [11, 12] was designed to have a smooth transition to the usual nonrelativistic potential model of NN interaction. This was achieved by using a substraction procedure to define the NN potential in the coupled $NN \oplus N\Delta \oplus \pi NN$ space from a chosen NN potential which fits the low energy NN data. The resulting model not only maintains the good fit to the low energy NN phase shifts, but can also describe the NN data up to about 1 GeV. Note however that the reproduction of the data is not perfect. Specifically, the description of the polarization cross sections is not ideal. Starting with such a coupled-channel model will make the present study significantly different from all of the previous studies of the Δ effect on the $NN\gamma$ reaction. In particular, we will be able to make realistic predictions in the intermediate energy region where extensive data will soon become available at COSY, the proton-cooler ring at the Forschungszentrum Juelich (Germany).

In the formulation of Refs. [11, 12], it is assumed that the Hamiltonian for NN scattering can be written in terms of three degrees of freedom: N, π, and Δ. In this work, we further assume that the $NN\gamma$ reaction can be described by adding to this Hamiltonian the electromagnetic interaction $V_{\rm em}$ introduced in Ref. [10]. The model Hamiltonian then takes the form

$$H = H_0 + H_{\rm int} + V_{\rm em}, \tag{1}$$

where H_0 is the sum of relativistic free energy operators, e.g., $\sqrt{p^2 + m_\alpha^2}$ for the $\alpha = N$, Δ, and π degrees of freedom. We will neglect the nonresonant pionic interactions (H_2' of Eq. (1.2) of Ref. [12]) which are found in Ref. [12] to be unimportant in describing NN scattering. The $N\Delta$ direct interaction is also neglected in Refs. [11, 12] for simplicity. The considered hadronic interaction is then of the following form:

$$H_{\rm int} = \sum_{i=1}^{2}[h_{\pi N,\Delta}(i) + h_{\Delta,\pi N}(i)] + \frac{1}{2}\sum_{i,j=1}^{2}[V_{NN,NN}(i,j) + V_{NN,N\Delta}(i,j) + V_{N\Delta,NN}(i,j)]. \tag{2}$$

The derivation of the NN scattering equation from the hadronic Hamiltonian $H_0 + H_{\rm int}$ can be found in Ref. [21] and was summarized in Ref. [12]. For our present purpose, we will neglect the much weaker effects due to the $N\Delta$ scattering (induced by the vertex interaction $h_{\pi N\leftrightarrow\Delta}$) and the coupling to the πd channel. The resulting scattering T matrix in the coupled $NN \oplus N\Delta$ space then takes the following form:

$$T_{NN,NN}(E) = \hat{V}_{NN,NN}(E) + \hat{V}_{NN,NN}(E)\frac{P_{NN}}{E - H_0 + i\epsilon} \times T_{NN,NN}(E), \tag{3}$$

$$T_{N\Delta,NN}(E) = V_{N\Delta,NN}\left(1 + \frac{P_{NN}}{E + H_0 + i\epsilon}T_{NN,NN}(E)\right), \tag{4}$$

$$T_{NN,N\Delta}(E) = \left(1 + T_{NN,NN}(E)\frac{P_{NN}}{E - H_0 + i\epsilon}\right)V_{NN,N\Delta}, \tag{5}$$

where the effective NN potential is

$$\hat{V}_{NN,NN}(E) = V_{NN,NN} + U^{(1)}_{NN,NN}(E), \tag{6}$$

with

$$U^{(1)}_{NN,NN}(E) = V_{NN,N\Delta}\frac{P_{N\Delta}}{E - H_0 - \Sigma_\Delta(E)}V_{N\Delta,NN}. \tag{7}$$

In the above equations, P_{NN} and $P_{N\Delta}$ are, respectively, the projection operators for the NN and $N\Delta$ channels. The Δ self-energy Σ_Δ is determined by the $h_{\pi N\leftrightarrow\Delta}$ vertex interaction in the presence of a spectator nucleon

$$\Sigma_\Delta(E) = \sum_{i=1}^{2} h_{\Delta,\pi N}(i)\frac{P_{\pi NN}}{E - H_0 + i\epsilon}h_{\pi N,\Delta}(i), \tag{8}$$

where $P_{\pi NN}$ is the projection operator for the πNN state. The vertex interaction $h_{\pi N\leftrightarrow\Delta}$ was determined from fitting the πN P_{33} phase shifts. The transition potential $V_{NN\leftrightarrow N\Delta}$ was taken from the one-pion-exchange model of Niephaus *et al.* [22] with a monopole form factor $(\Lambda^2 - m_\pi^2)/(\bar{q}^2 + \Lambda^2)$ ($\bar{q}$ denotes the three-momentum

transfer). The NN interaction is defined by a subtraction of *any* NN potential which fits the NN phase shifts below the pion production threshold. In this work we consider the Paris potential [23] and hence the NN interaction in Eq. (6) is defined by

$$V_{NN,NN} = V_{\rm Paris} - U^{(1)}(E = E_s), \tag{9}$$

where the substraction energy E_s is a parameter. The above definition of the NN interaction amounts to removing phenomenologically the two-pion exchange with an intermediate $N\Delta$ state from the Paris potential, in order to avoid the double counting of the $N\Delta$ effect. In Refs. [11, 12], it was found that by choosing $\Lambda = 650$ (MeV/c) and $E_s = 10$ MeV (the laboratory energy of the incident nucleon) the solution of Eq. (3) can best reproduce the phase shifts calculated from the Paris potential at energies below about 300 MeV, and can also describe the NN phase shifts reasonably well up to about 1 GeV.

The numerical method for solving the above coupled-channel equations (3)–(9) in the momentum-space representation was well developed in Refs. [11, 12]. The calculated plane-wave matrix elements of $T_{NN,NN}(E)$, $T_{NN,N\Delta}(E)$, and $T_{N\Delta,NN}(E)$ are the input to the study of the $NN\gamma$ reaction. The formalism presented above yields T matrices which are a solution of the nonrelativistic Schrödinger equation. Thus the expression for the NN cross section calculated with these T matrices is

$$\frac{d\sigma}{d\Omega} = \frac{m_N^2}{4\pi}|T_{NN,NN}(E)|^2, \tag{10}$$

where m_N denotes the nucleon mass.

The coupled-channel $NN \oplus N\Delta \oplus \pi NN$ model described briefly above is undoubtedly not fully relativistic. Unfortunately, this deficiency cannot be easily removed because of the complexities of the NN interactions in the Δ excitation region. It also contains some model dependences which were investigated in some detail in Ref. [11]. In particular, the choice of the starting low energy potential and the parametrization of the $NN \leftrightarrow N\Delta$ potential is not unique. Similar to all of the low energy NN potentials, this is an unavoidable phenomenology. The choice can only be determined by finding out which combination can best reproduce all of the NN data. It turned out that the use of the Paris potential and the $NN \leftrightarrow N\Delta$ potential of Niephaus *et al.* [22] gave the best NN results. Furthermore, the use of the Δ self-energy, defined in Eq. (8), is crucial in obtaining a good fit to the NN phase shifts, as emphasized in Ref. [11]. As seen in Ref. [12], the use of other low energy potentials did not yield better NN results. For our present purposes, we therefore use the model of Ref. [11] as described above. It remains to be seen whether this model can account for a unified description of both the NN scattering and NN bremsstrahlung process.

Before we proceed further, it is necessary to define the electromagnetic interaction $V_{\rm em}$ of Eq. (1). For the $pp \to pp\gamma$ reaction, it is sufficient to only consider the one-baryon currents since the leading term of the two-body current is absent in the $pp\gamma$ reaction. Similar to the approach developed in Ref. [24] to study the electromagnetic production of pions, the one-baryon current operator introduced in Ref. [10] is defined by the matrix elements of the Feynman amplitudes calculated from an effective Lagrangian. In this way we include the important relativistic spin correction into our model. The matrix element of the electromagnetic transition potential is then given by

$$\langle \vec{p}', \vec{k}\,\lambda|V_{\rm em}|\vec{p}\rangle = \sqrt{\frac{m_\alpha}{E^\alpha_{p'}}}\langle \vec{p}', \vec{k}\,\lambda|\tilde{V}_{\rm em}|\vec{p}\rangle\sqrt{\frac{m_{\alpha'}}{E^{\alpha'}_{p}}}, \tag{11}$$

where $\langle \vec{p}'\,\vec{k}, \lambda|\tilde{V}_{\rm em}|\vec{p}\rangle$ denotes the Lorentz-invariant matrix element and $E^\alpha_p = \sqrt{p^2 + m^2_\alpha}$. For the $N \leftrightarrow N\gamma$ vertex this is ($\vec{k} + \vec{p}' = \vec{p}$)

$$\langle \vec{p}', \vec{k}\,\lambda|\tilde{V}_{\rm em}|\vec{p}\rangle$$

$$= \bar{u}(\vec{p}')\left(-ie_i \not{\epsilon} + \frac{(\mu_i - 1)e}{4m}(\not{k}\not{\epsilon} - \not{\epsilon}\not{k})\right)u(\vec{p}), \tag{12}$$

where λ denotes a photon state with polarization ϵ_μ. We follow the conventions of Bjorken and Drell [25]. The nucleon Dirac spinor is denoted as $u(\vec{p})$, normalized as $\bar{u}(\vec{p})u(\vec{p}) = 1$. The charge and anomalous magnetic moment of the ith nucleon are denoted, respectively, by e_i and μ_i. Similarly, the matrix elements of the $N \to \gamma\Delta$ and $\Delta \to \gamma N$ vertex interactions are, respectively,

$$\langle \vec{p}_\Delta, \vec{k}\,\lambda|\tilde{V}_{\rm em}|\vec{p}\rangle = \bar{\psi}^\mu(\vec{p}_\Delta)\Gamma^{\Delta N\gamma}_\mu u(\vec{p}) \tag{13}$$

and

$$\langle \vec{p}, \vec{k}\,\lambda|\tilde{V}_{\rm em}|\vec{p}_\Delta\rangle = \bar{u}(\vec{p})\Gamma^{N\Delta\gamma}_\mu \psi^\mu(\vec{p}_\Delta), \tag{14}$$

where $\psi^\mu(\vec{p}_\Delta)$ is the Rarita-Schwinger spinor with normalization $\bar{\psi}^\mu(\vec{p})\psi_\mu(\vec{p}) = -1$. We follow Jones and Scadron [26] to write the gauge-invariant vertex functions

$$\Gamma^{N\Delta\gamma}_\mu = K^1_\mu + K^2_\mu \tag{15}$$

with

$$K^1_\mu = -ieG_1(\not{k}\epsilon_\mu - \not{\epsilon}k_\mu)\gamma^5 T_z, \tag{16}$$

$$K^2_\mu = -ieG_2(\epsilon_\mu P\cdot k - \epsilon\cdot P k_\mu)\gamma^5 T_z. \tag{17}$$

For the decay of a Δ in a nucleon and photon we have

$$\Gamma^{\Delta N\gamma}_\mu = -K^1_\mu + K^2_\mu. \tag{18}$$

In the above expressions $k_\mu = p^{\rm in}_\mu - p^{\rm out}_\mu$ is the photon momentum (defined to be outgoing from the vertex) and $P = \frac{1}{2}(p^\Delta_\mu + p^N_\mu)$. T_z is the third component of the isospin transition matrix for coupling an isospin 3/2 to an isospin 1/2 particle.

The coupling constants G_1 and G_2 in Eqs. (16) and (17) are conventionally determined by fitting to the $M1^+$ and $E1^+$ multipole data on the photoproduction of pions from nucleons [24, 26–29]. The values obtained depend on the treatment of the nonresonant background contributions. Although this leads to some uncertainty in the values, the parameters found in the literature are not too far apart. It has also been shown [28, 29] that in order to accurately reproduce the $M1^+$ multipole data on the pion photoproduction around the resonance energy, one needs energy-dependent couplings G_1 and G_2. However,

given the uncertainty in the coupling constants we ignore this dependence. Bearing in mind that the vertex K_μ^1 gives the dominant contribution, we can classify the various sets of coupling constants by the magnitude of G_1. The lowest value is found by Nozawa *et al.* [24]: $G_1 = 2.024$ (GeV^{-1}) and $G_2 = -0.851$ (GeV^{-2}). Highest values are given by Jones and Scadron [26]: $G_1 = 2.68$ (GeV^{-1}) and $G_2 = -1.84$ (GeV^{-2}) and by Davidson *et al.* [27]: $G_1 = 2.556$ (GeV^{-1}) and $G_2 = -1.62$ (GeV^{-2}). Note that the authors of Ref. [27] have a slightly different definition of K_2. An alternative way to extract the $N\Delta\gamma$ coupling parameters is to assume vector-meson dominance. On the $N\Delta\gamma$ vertex only the isospin-1 vector meson contributes and the coupling strengths are determined by the ratio of $g_{\rho NN}$ and $g_{\rho N\Delta}$. Using the coupling constants of Ref. [30] this procedure gives $G_1 = 2.0$ (GeV^{-1}) and $G_2 = 0$ (GeV^{-2}), comparable with the values from pion photoproduction.

The above parametrization of the $\gamma N \leftrightarrow \Delta$ vertex is for the case that both the nucleon and the Δ are on their mass shell; i.e., $p_0 = \sqrt{m^2 + p^2}$ and only the positive-energy spinors are retained. We then have the Rarita-Schwinger condition $\gamma^\mu \psi_\mu(\bar{p}) = 0$ and the off-shell parameters discussed in Refs. [31–33] will not occur. This simplification is consistent with our Hamitonian formulation defined in this section. The extension of our approach to include the off-mass-shell dependence requires a reconstruction of the coupled-channel $NN \oplus N\Delta \oplus \pi NN$ model. This is beyond the scope of this work. It is certainly a possible improvement for future investigations.

In the description of NN bremsstrahlung reactions, where the calculations are based on NN-potential models, one makes use of the Lorentz-invariant nature of the various $NN\gamma$ transition amplitudes describing different bremsstrahlung processes. It is then important to be able to obtain such invariant amplitudes from potential models that are based on nonrelativistic approaches, which yield Galilean invariant amplitudes. This is the case of the present model given by Eqs. (1)–(9). In Ref. [5] a procedure is described to construct Lorentz-invariant amplitudes from nonrelativistic amplitudes. Following this prescription we construct an amplitude that transforms covariantly by including the proper E/m factors and using the proper relativistic kinematics. This procedure is similar to the introduction of "minimal relativity" in earlier studies of relativistic effects on nuclear bound states [34]. However, although the procedure provides us with matrix elements that transform covariantly, our formulation is not fully relativistic. It suffers from the inconsistency commonly encountered in constructing realistic meson-exchange NN models. This deficiency is unavoidable in practice since we do not have a reliable relativistic theory for describing the short-range interactions which are clearly beyond the meson-exchange description. We also point out that our formalism is equivalent to what one obtains when starting out from a field-theoretic point of view and (a) approximates all propagators by their positive energy content, and (b) applies a three-dimensional Thompson-like reduction to all integrations over the four-momentum.

With the "minimal relativity" prescription, and in first order of the electromagnetic coupling, the Lorentz-invariant amplitude of the $pp \to pp\gamma$ reaction defined by the model Hamiltonian Eq. (1) is

$$\langle pp\gamma|\tilde{M}(E)|pp\rangle = \langle pp\gamma|\tilde{M}^{\rm ext}|pp\rangle + \langle pp\gamma|\tilde{M}^{\rm resc}|pp\rangle, \tag{19}$$

where the external, or single-scattering, term is

$$\langle pp\gamma|\tilde{M}^{\rm ext}|pp\rangle = \sum_{\alpha=N,\Delta} \langle pp\gamma|\tilde{V}_{\rm em}|\alpha\rangle G_\alpha(E)\langle\alpha|\tilde{T}_{N\alpha,NN}(E)|pp\rangle$$
$$+ \sum_{\alpha=N,\Delta} \langle pp|\tilde{T}_{NN,N\alpha}(E-E_\gamma)|\alpha\rangle G_\alpha(E-E_\gamma)\langle\gamma\alpha|\tilde{V}_{\rm em}|pp\rangle. \tag{20}$$

E_γ is the photon energy and we have introduced the N and Δ propagators ($E_p^N = \sqrt{p^2 + m_N^2}$, etc.)

$$G_N(W) = \frac{m_N}{E_p^N} \frac{1}{p_0 - E_p^N + i\epsilon}, \tag{21}$$

$$G_\Delta(W) = \frac{m_\Delta^*}{E_p^{\Delta *}} \frac{1}{p^0 - E_p^\Delta - \frac{m_\Delta}{E_p^\Delta}\Sigma^\Delta(p^0,\bar{p})}, \tag{22}$$

where $p_0 = W - E_{p_1}$, the energy available for propagation in the presence of the spectator particle, which has momentum $\bar{p}_1$. $\tilde{T}_{NN,N\alpha}$ denotes the Lorentz-invariant scattering amplitude, constructed from $T_{NN,N\alpha}$ by [5]

$$\langle\bar{p}'|\tilde{T}_{NN,N\alpha}|\bar{p}\rangle = \left(\frac{E_p^N}{m_N}\right)^{1/2}\left(\frac{E_{p'}^N}{m_N}\right)^{1/4}\left(\frac{E_{p'}^{\alpha *}}{m_\alpha^*}\right)^{1/4}\langle\bar{p}'|T_{NN,N\alpha}|\bar{p}\rangle. \tag{23}$$

The rescattering term is

$$\langle pp\gamma|\tilde{M}^{\rm resc}|pp\rangle = \sum_{\alpha,\beta,\delta=N,\Delta} \langle pp|\tilde{T}_{NN,\delta\beta}(E-E_\gamma)|\delta\beta\rangle G_{\delta\beta}(E-E_\gamma)\langle\gamma\delta|\tilde{V}_{\rm em}|\alpha\rangle G_{\alpha\beta}(E)\langle\delta\beta|\tilde{T}_{\alpha\beta,NN}(E)|pp\rangle$$

with

$$G_{\delta\beta}(E-E_\gamma)G_{\alpha\beta}(E) = R^{\alpha}_{p_1}R^{\beta}_{p_2}R^{\delta}_{p_3}\frac{1}{E-E_\gamma-\tilde{E}^{\delta}_{p_3}-\tilde{E}^{\beta}_{p_2}}\frac{1}{E-\tilde{E}^{\alpha}_{p_1}-\tilde{E}^{\beta}_{p_2}},$$

$$R^N_p = \frac{m_N}{E^N_p},\quad R^\Delta_p = \frac{m^*_\Delta}{E^{\Delta*}_p},\quad \tilde{E}^N_p = E^N_p,\quad \tilde{E}^\Delta_p = E^\Delta_p - \frac{m_\Delta}{E^\Delta_p}\Sigma^\Delta(p^0,\vec{p}). \tag{24}$$

In the above equations $m^*_\Delta = 1.23$ GeV is the physical mass of the Δ, and m_Δ is the bare mass of the Δ. Also $E^{\Delta*}_p = \sqrt{p^2+m^{*2}_\Delta}$ and $E^\Delta_p = \sqrt{p^2+m^2_\Delta}$. The Δ propagator we use is consistent with the relativistic extension of the Δ propagator used in Ref. [30]. The specific form of $\Sigma^\Delta(p^0_\Delta,\vec{p}_\Delta)$ determines the value of the bare Δ mass due to the requirement that the Δ propagator is resonant at the physical resonance position, $p^0_\Delta = m^*_\Delta$. The form of Σ_Δ is restricted by the P_{33} phase shift. However, one finds satisfactory reproductions of the P_{33} phase shift with rather different forms of Σ^Δ. For example, the Bransden-Moorhouse parametrization only has an imaginary part of the self-energy, implying $m^0_\Delta = m^*_\Delta$. In the approach of ter Haar and Malfliet [30] one gets $m^0_\Delta = 1.46$ GeV. Lee [11] reports an accurate reproduction of the P_{33} phase shift over a large energy range for a value $m^0_\Delta = 1.28$ GeV. As we will show later, the form of Σ^Δ has a definite influence on the magnitude of the Δ decay diagrams.

In the calculation of Eq. (24) we neglect the terms where more than one of the intermediate particles is a Δ. Thus we do not include diagrams with a two-Δ propagator which is expected to be small due to the mass difference. The diagrams with a $\Delta\Delta\gamma$ coupling are also not included in this work, mainly because the experimental information of $\Delta\Delta\gamma$ coupling is still limited (only from the analysis of very limited data of a complex experiment on $\pi N \to \pi N\gamma$; see, for example, the work by Heller *et al.* [35]). This will minimize the model dependence of our predictions. It is in fact one of our hopes that the differences between the results from our approach and the forthcoming data can provide some information about the $\Delta\Delta\gamma$ coupling which can be used to test various QCD-inspired models of the Δ. This however cannot be meaningfully explored unless our approach is further improved to account for the deficiencies mentioned before.

The various processes contributing to the $NN\gamma$ reaction defined by Eqs. (20)–(24) are illustrated in Fig. 1. They can be classified as (1) the contributions from the nucleon current [Figs. 1(a) and 1(b)], (2) the contributions from the direct Δ decay [Fig. 1(c)], and (3) the contributions from the $N\Delta$ rescattering [Fig. 1(d)]. Note that the NN and $N\Delta$ T matrix in each diagram is determined by different collision energies since the outgoing photon shares the total energy available to the system. This complicates the calculation if we follow the conventional approach based on the partial-wave decomposition. Instead, we directly carry out the calculation of the diagrams with a $N\Delta\gamma$ vertex in a plane-wave basis. The plane-wave T matrices are constructed from the partial-wave solutions of Eqs. (3)–(9) by including partial waves up to $J = 9$. Calculating in the plane-wave basis allows an exact treatment of the relativistic features such as that of the vertex interactions defined by Eqs. (12)–(18).

With the "minimal relativity" prescription described previously, all matrix elements of the $pp\gamma$ process displayed in Fig. 1 are Lorentz invariant. We therefore are allowed to calculate each of them in any convenient frame. The calculation of the contributions from the nucleon current [Figs. 1(a) and 1(b)] is identical to that of Ref. [5], except that the NN T matrix is now generated from the coupled-channel equations (3)–(9). By setting the coupling term $U^{(1)}$ in Eqs. (3) and (9) to zero, we reproduce the results of Ref. [5]. For the single-scattering Δ-decay diagrams [Fig. 1(c)], it is most convenient to do the calculation in the c.m. frame of the initial NN state. Explicitly, from Eq. (20) we have for this diagram

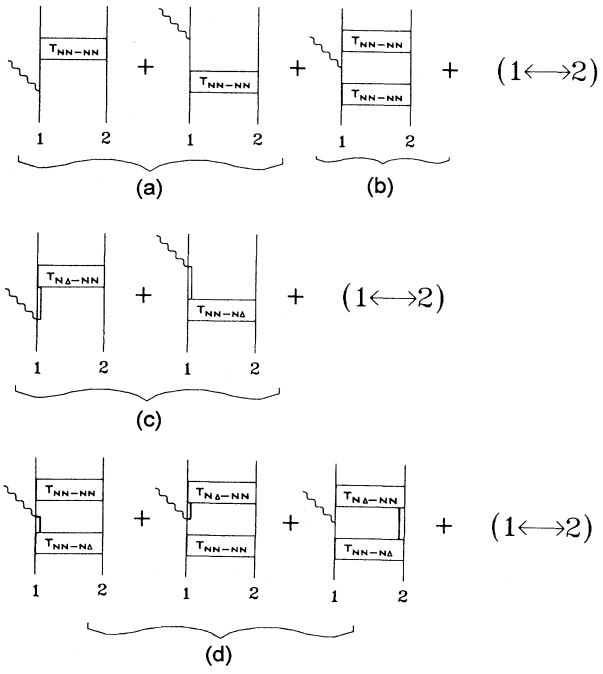

FIG. 1. Diagrams included in the calculation (a single line denotes a nucleon, a double line a Δ intermediate state): single-scattering diagrams with T_{NN-NN} (a), rescattering diagrams with T_{NN-NN} (b), single-scattering diagrams with $T_{NN-N\Delta}$ (c), and rescattering diagrams with $T_{NN-N\Delta}$ (d).

$$\tilde{M}^{\rm ext}(r_1,r_2,r_1',r_2') = \sum_{r''} \langle \bar{p}'', r_1' | \tilde{\Gamma}^{\Delta N\gamma} | \bar{p}', r_1'' \rangle \frac{m_\Delta^*}{E_{p'}^{\Delta *}} \frac{1}{p_0^\Delta - E_{p'}^\Delta - \frac{m_\Delta^0}{E_{p'}^\Delta}\Sigma^\Delta(p_0^\Delta,\bar{p}')}$$
$$\times \langle \bar{p}', r_1'', r_2' | \tilde{T}_{N\Delta,NN}(s = 4E_p^{N\,2}) | \bar{p}, r_1, r_2 \rangle$$

with

$$\langle \bar{p}'', r_1' | \tilde{\Gamma}^{\Delta N\gamma} | \bar{p}', r_1'' \rangle = \bar{u}_{r_1'}(\bar{p}'') \Gamma_\mu^{\Delta N\gamma} \psi_{r_1''}^{\mu *}(\bar{p}),$$
$$\langle \bar{p}', r_1'', r_2' | \tilde{T}_{NN,N\Delta}(s) | \bar{p}, r_1, r_2 \rangle = \bar{\psi}_{r_1''}^{\mu *}(\bar{p}') \bar{u}_{r_2'}(-\bar{p}') \tilde{T}_\mu^{N\Delta,NN}(s) u_{r_1}(\bar{p}) u_{r_2}(-\bar{p}),$$
$$p_0^\Delta = 2E_p^N - E_{p'}^N. \tag{25}$$

In these equations r denotes the spin index of the respective spinor, $\Gamma_\mu^{\Delta N\gamma}$ is defined in Eq. (18), the momenta $\bar{p}$,$\bar{p}'$ and $\bar{p}''$ are determined by the external kinematics. A similar expression is found for the second diagram of Fig. 1(c) where the photon is emitted before the strong interaction.

The expressions for the rescattering diagrams with Δ's are evaluated in the same fashion. We see from Eq. (24) that the calculation involves an integration over the intermediate state. Again we use the Lorentz invariance of the $pp\gamma$ amplitude and evaluate the diagram in a suitable frame. We find for the rescattering diagram where a nucleon is excited into a Δ and a real photon

$$\tilde{M}_{N\Delta\gamma}^{\rm resc} = \int \frac{d\bar{p}''}{(2\pi)^3} \sum_{r_1'',r_2'',r_3'''} \left\langle \bar{p}' - \frac{\bar{k}}{2}, r_1', -\bar{p}' - \frac{\bar{k}}{2}, r_2' \left| \tilde{T}_{NN,\Delta N}[s = (E_{\bar{p}'-\frac{\bar{k}}{2}}^N + E_{-\bar{p}'-\frac{\bar{k}}{2}}^N)^2 - \bar{k}^2] \right| \bar{p}'' - \bar{k}, r_1''', -\bar{p}'', r_2'' \right\rangle$$
$$\times \left(\frac{m_N^2}{E_{p''}^{N\,2}} \frac{m_\Delta^*}{E_{\bar{p}''-\bar{k}}^{\Delta *}} \right) \left(\frac{1}{2E_p^N - 2E_{p''}^N} \right) \left(\frac{1}{2E_p^N - k_0 - E_{p''}^N - E_{\bar{p}''-\bar{k}}^{\Delta *} - \frac{m_\Delta^0}{E_{\bar{p}''-\bar{k}}^\Delta}\Sigma^\Delta(p_0^\Delta,\bar{p}''-\bar{k})} \right)$$
$$\times \langle \bar{p}'' - \bar{k}, r_1''' | \tilde{\Gamma}^{N\Delta\gamma} | \bar{p}'', r_1'' \rangle \langle \bar{p}'', r_1'', r_2'' | \tilde{T}^{NN,NN}(s = 4E_p^{N\,2}) | \bar{p}, r_1, r_2 \rangle,$$
$$p_0^\Delta = E_p^N - k_0. \tag{26}$$

In this expression k is the photon momentum. The notation is similar to Eq. (25); we specified explicitly all the momenta of the ΔN T matrix which is not in its c.m. frame. Due to the presence of the (complex) Δ self-energy the denominator with Σ^Δ has no zero in the region of integration. The other denominator does have a zero, evaluating the diagram in the c.m. frame of the NN T matrix allows the pole to be treated with a simple subtraction method. The other rescattering diagrams with a Δ intermediate state are calculated in the same manner.

Finally we point out that the rescattering diagram where the Δ is the spectator has an intermediate state which separates in a proton-Δ^+ and a neutron-Δ^{++} state. The photon couples to the nucleon, hence this diagram has a contribution depending on the magnetic moment of the neutron. This contribution is gauge invariant, however the contribution of the proton-proton-photon vertex is not. Also, since the introduction of Δ intermediate states allows for the exchange of charged mesons in the proton-proton T matrix, meson-exchange currents (MEC's) will be nonzero. This all shows that the inclusion of Δ intermediate states has implications on the gauge invariance of the model. The present model is gauge invariant only in the soft-photon approximation, as are all existing potential model calculations (even those which do not consider the subnucleonic degrees of freedom). In order to fulfill the gauge-invariance condition of the existing potential model calculations in general, and the present calculation in particular, one needs to take into account contributions of the effective two-body current, especially those processes involving antiparticle propagations (pair diagrams). This is beyond the scope of the present work.

III. RESULTS

In this section, we will first present results in the low energy region where the experimental data at $E_{\rm lab} = 280$ MeV are available. We then present our predictions at $E_{\rm lab} = 550$ MeV for the forthcoming experimental test at COSY. We will also consider the kinematic region where the Δ dynamics can be best studied.

Compared with the previous works in the low energy region ($E_{\rm lab} \leq$ about 300 MeV), an important feature of our approach is that we calculate the T matrices $T_{NN,NN}$ and $T_{NN\leftrightarrow N\Delta}$ from a coupled-channel model which was obtained by extending the Paris potential to include the coupling with the $N\Delta$ and πNN states. As shown in Refs. [11, 12] and briefly discussed in Sec. II, the constructed coupled-channel model is as good as the Paris potential in describing the NN data in the low energy region below the pion production threshold. In order to illustrate the on- and off-shell differences between the NN interaction based on the Paris potential and our coupled-channel approach, we decompose the NN T matrix in its spin-isospin compenents [36]:

$$\langle \vec{p}'|T_{NN,NN}|\vec{p}\rangle = \left[\alpha_1 P_{S=0} + \alpha_2 P_{S=1} + i\alpha_3(\vec{\sigma}_1+\vec{\sigma}_2)\cdot\hat{n} + \alpha_4 S_{12}(\hat{q}) + \alpha_5 S_{12}(\hat{Q}) + \alpha_6 S_{12}(\hat{q},\hat{Q})\right] P_T, \tag{27}$$

where

$$\hat{q} = \frac{\vec{p}-\vec{p}'}{|\vec{p}-\vec{p}'|}, \quad \hat{Q} = \frac{\vec{p}+\vec{p}'}{|\vec{p}+\vec{p}'|}, \quad \hat{n} = \frac{\vec{p}\times\vec{p}'}{|\vec{p}\times\vec{p}'|},$$
$$P_{S=0} = \frac{1}{4}(1-\vec{\sigma}_1\cdot\vec{\sigma}_2), \quad P_{S=1} = \frac{1}{4}(3+\vec{\sigma}_1\cdot\vec{\sigma}_2),$$
$$S_{12}(\hat{p}) = 3\vec{\sigma}_1\cdot\hat{p}\vec{\sigma}_2\cdot\hat{p} - \vec{\sigma}_1\cdot\vec{\sigma}_2,$$
$$S_{12}(\hat{p}',\hat{p}) = \frac{3}{2}(\vec{\sigma}_1\cdot\hat{p}'\vec{\sigma}_2\cdot\hat{p} + \vec{\sigma}_1\cdot\hat{p}\vec{\sigma}_2\cdot\hat{p}') - \hat{p}'\cdot\hat{p}\vec{\sigma}_1\cdot\vec{\sigma}_2. \tag{28}$$

The first two terms in Eq. (27), proportional to the spin projection operator $P_{S=0}$ and $P_{S=1}$, are the central spin-single ($S=0$) and spin-triple ($S=1$) components, respectively. The third term is the spin-orbit component, the fourth and fifth terms are the usual tensor components. The last term in Eq. (27) is the off-shell tensor component which vanishes identically on shell as a consequence of time-reversal invariance. P_T in Eq. (27) denotes the total isospin projection operator. For proton-proton scattering, it projects out onto the total isospin $T=1$ subspace. In Fig. 2 we compare the NN on-shell interaction. Here, following Ref. [37], we show the angle-averaged magnitude of each spin-isospin compenent with total isospin $T=1$. The dashed curves are the results for the Paris potential while the solid curves stand for the coupled-channel model results. The only notable differences are in the $P_{S=1}$ channel. The small differences seen in Fig. 2 are expected since the subtraction method defined by Eq. (9) yields a correction $U^{(1)}(E) - U^{(1)}(E_s)$ to the Paris potential, which is very small at low energies and becomes significant only as the collision energy approaches the pion production threshold.

The main difference between the Paris potential and the coupled-channel model is in the off-shell T matrices which describe the wave functions in the interaction region. As an example, we compare in Fig. 3 the half-off-shell T matrices calculated from these two models at $E_{\rm lab} = 280$ MeV as a function of the off-shell momentum $p' = |\vec{p}'|$. Significant differences can be observed in most of the channels, especially at higher off-shell momenta. However, the $pp\gamma$ reaction at this low energy only probes the low momentum region ($p' \leq 0.36$ GeV/c) in which the differences between the two half-off-shell T matrices are much smaller. Moreover, the $pp\gamma$ reaction is insensitive to the central $P_{S=0}$ channel [38], which shows the largest difference in Fig. 3. We compare in Fig. 4 the $NN\gamma$ analyzing powers predicted by the Paris potential (dashed curve) and the coupled-channel model (solid curve), for proton angles of 12.4° and 14.0° at $E_L = 280$ MeV. To emphasize the farthest off-shell region, we did not include the rescattering mechanisms [Figs. 1(b) and 1(d)] in this calculation. Obviously, the off-shell differences shown in Fig. 3 do not lead to any dramatic effects on the $NN\gamma$ reaction at low energies. We mention that the analyzing power is most sensitive to the tensor and central spin-triple components of the NN interaction [37].

We now turn to analyzing the effect due to the Δ mechanism which was found in Ref. [10] to be significant already at $E_L = 280$ MeV. At certain kinematic conditions, the Δ mechanism can increase the cross section up to 30%. But it can decrease, less substantially, the cross section at other kinematic conditions. Clearly there is a very large interference effect due to the presence of the Δ excitation. The Δ current, which is almost exclusively magnetic, interferes very effectively with the magnetic part of the nuclear current. The latter gives the dominant contribution at this energy. To see how

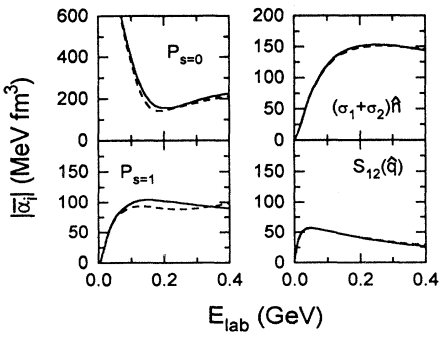

FIG. 2. Magnitude of the spin-isospin components of the on-shell interaction, averaged over the scattering angle as a function of the laboratory energy. The solid line stands for the T matrix including Δ intermediate states, the dashed line represents the Paris T matrix.

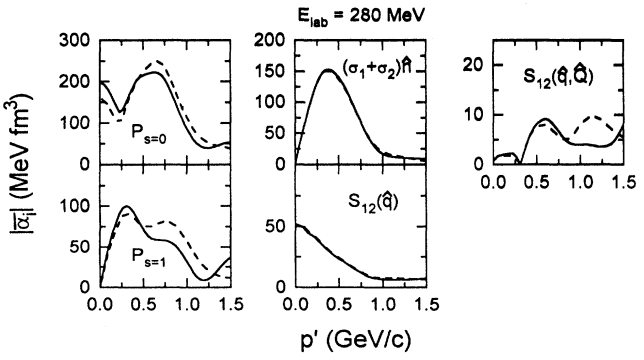

FIG. 3. Magnitude of the spin-isospin components of the half-off-shell interaction, averaged over the scattering angle as a function of the off-shell momentum at a beam energy $E_{\rm lab}$ = 280 MeV. The solid line stands for the T matrix including Δ intermediate states, the dashed line represents the Paris T matrix.

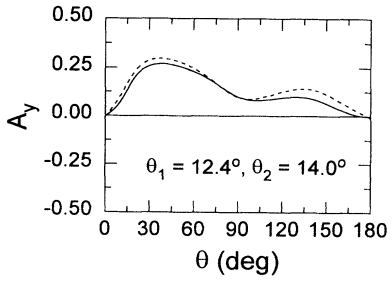

FIG. 4. Coplanar analyzing power for proton-scattering angles $\theta_1 = 12.4$ and $\theta_2 = 14.0$ as a function of the photon angle, $E_{\rm lab} = 280$ MeV. The solid line is the result [including the nucleon single-scattering diagram, Fig. 1(a)] calculated with the T matrix with Δ intermediate states, the dashed line is obtained using the Paris T matrix.

this arises within our model, we present in Fig. 5 the results at $E_{\rm lab} = 280$ MeV calculated from various combinations of single-scattering mechanisms [Figs. 1(a) and 1(c)]. We first observe that at this low energy the contribution from the Δ excitation alone (dot-dot-dashed curve) is less than 10% of the contribution from the nucleon current (dot-dashed curve). The Δ contribution depends only very weakly on the photon angle, while the nucleonic contribution shows a large variation. Second, we note that the Δ contribution [Fig. 1(c)] consists of two different amplitudes: (1) the preemission amplitude due to the emission of the proton before the strong interaction takes place, (2) the postemission amplitude due to the emission of the photon after the NN collision. The difference between these two amplitudes is mainly in the $\gamma N\Delta$ vertex. The preemission amplitude is determined by the vertex $\Gamma^{\gamma N\Delta}$, and the postemission amplitude by $\Gamma^{\gamma\Delta N}$. From expressions (15) and (18), we see that the dominant K^1_μ term of the preemission vertex $\Gamma^{\gamma\Delta N}$ has a minus sign relative to that of the postemission vertex $\Gamma^{\gamma N\Delta}$. Consequently, the preemission and postemission amplitudes tend to have opposite effects in interfering with the nucleonic contribution. This is also illustrated in Fig. 5. It is seen that when the premission amplitude is added to the nucleonic amplitude, the interference effect is destructive at all angles and yields the dashed curve in Fig. 5. On the other hand, the interference due to the postemission of Δ is constructive. By further adding this amplitude to the calculation, the result is shifted from the dashed curve to the solid curve. This sensitive interference between the nucleonic and Δ contribution provides an opportunity to test our model of the Δ excitation.

In calculating the Δ contributions to the $NN\gamma$ reaction it is crucial to use a Δ propagator which is consistent with the T matrices used. As discussed in Sec. II, there are other forms of the Δ self-energy found in the literature. All are constrained by fitting the πN phase shifts in the P_{33} channel, but results from different formulations of πN scattering. To use these different parametrizations of the Δ self-energy, it is necessary to readjust the other parts of the considered coupled-channel model such that the good fit to the NN phase shifts is maintained. This is a nontrivial task, but is an important model dependence we should address in the future. To get some insight into the sensitivity of our predictions to this phenomenological part of the model, we show in Fig. 6 a result from our calculation (dashed curve) using Eq. (8) to determine the Δ self-energy and a result (solid curve) using the self-energy of ter Haar and Malfliet [30]. The contributions of the nucleonic current are represented by the dotted curve. In all calculations the same T matrices based on the Paris potential including Δ intermediate states were used. Although both propagators fit the P_{33} phase shift,

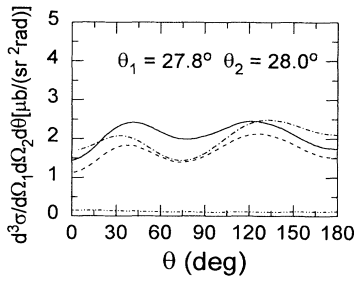

FIG. 5. The various contributions to the total cross section, in a coplanar geometry with proton-emission angles $\theta_1 = 27.8$ and $\theta_2 = 28.0$, $E_{\rm lab} = 280$ MeV. No rescattering contributions were included. The dash-dotted line is the result with only the nucleon contributions [Fig. 1(a)], the solid line stands for the full model [Figs. 1(a) and 1(c)] taking the high $N\Delta\gamma$ coupling set [$G_1 = 2.68$ (GeV^{-1}), $G_2 = -1.84$ (GeV^{-2})]. The dashed line stands for the nucleonic contributions plus the preemission diagrams. The dot-dot-dashed line is the result with only Δ-decay diagrams [Fig. 1(c)].

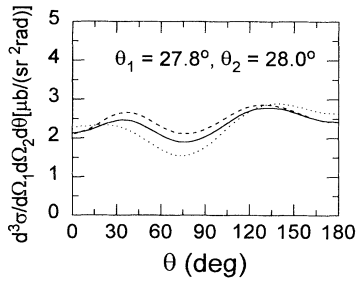

FIG. 6. The effect of the choice of the Δ propagator, in a coplanar geometry with proton-emission angles $\theta_1 = 27.8$ and $\theta_2 = 28.0$, $E_{\rm lab} = 280$ MeV. The dotted line is the result with only the nucleon contributions [Fig. 1(a)], the solid line is the result, including all diagrams, calculated with the Δ self-energy of ter Haar and Malfliet [30], the dashed line is the same calculation but using the Δ self-energy of Eq. (8). In these calculations we took $G_1 = 2.0$ (GeV^{-1}) and $G_2 = 0$ (GeV^{-2}).

the rather large difference between the results show the need to use a consistent Δ propagator. The observed difference is not difficult to understand. Because the self-energy is an analytic function, the energy-dependent imaginary part is accompanied by an energy dependence of the real part. At the energies under consideration ($E_{\rm lab}$ = 280 MeV) the invariant mass of the intermediate Δ is much smaller than the on-shell value of 1.23 GeV. At these values, the Δ self-energy is much smaller than the value at resonance. This enlarges the denominator of the Δ propagator, resulting in an additonial quenching of the Δ propagator. However, the effect is different for both self-energies considered above. The self-energy of ter Haar changes from an on-shell value of −230 MeV to −100 MeV far off shell; the respective numbers for the self-energy of Lee are −50 MeV and −20 MeV. Consequently, the Δ propagator is more quenched when using the self-energy of ter Haar. In view of this, all of the results presented hereafter are obtained using the self-energy of Eq. (8) in calculating the Δ propagator Eq. (22).

The inclusion of the Δ rescattering diagrams [Fig. 1(d)] is one of the main new features of this work. It provides an additional contribution due to the Δ excitation. In Fig. 7, we illustrate its effects at various laboratory energies in changing the calculated differential cross sections and analyzing powers. The contribution from the nucleonic currents alone is denoted by the dotted curves. By adding the Δ single-scattering mechanism [Fig. 1(c)], we obtain the dashed curves. The solid curves are obtained when the Δ rescattering mechanisms [Fig. 1(d)] are also included. At lower energies the effect of the Δ rescattering on the analyzing power is comparable to that of the Δ single-scattering mechanism. The contribution of the Δ rescattering to the cross section is about one-half of the single-scattering mechanism. At higher energies the rescattering diagrams are less significant. We have found that the largest Δ effect is due to the rescattering diagram where the Δ is a spectator [the rightmost diagram in Fig. 1(d)]. The calculation of this mechanism involves an integration over two half-off-shell $T_{NN\leftrightarrow N\Delta}$ matrices and hence is most sensitive to the short-range behavior of the transition potential $V_{NN\leftrightarrow N\Delta}$ used in solving the coupled equations (3)–(9). In the construction of Refs. [11, 12], the model of $V_{NN\leftrightarrow N\Delta}$ derived by Niephaus *et al.* [22] is used. Because of the use of a different regularization of the short-range part of the one-pion exchange, this model is rather different from the model employed in the $NN\gamma$ calculation of Ref. [10]. Consequently, the resulting effect of Δ rescattering is rather different. The Δ rescattering effect calculated using the $T_{NN\leftrightarrow N\Delta}$ matrices employed in Ref. [10] is much smaller in changing the differential cross sections. This is also the reason why the structure of the Δ contributions to the analyzing power at 280 MeV in the present work differs from the results found in Ref. [10]. We hope that the new high-precision measurements scheduled at the CELSIUS facility in Uppsala (Sweden) and the COSY ring in Juelich (Germany) will shed more light on this issue.

In Figs. 8 and 9, we compare our results with the experimental data at $E_{\rm lab}$ = 280 MeV. All mechanisms in Fig. 1 are included in the calculations. The scattering T matrices and the Δ self-energy needed in evaluating the γNN amplitudes defined by Eqs. (19)–(22) are generated from the model of Refs. [11, 12], as discussed in Sec. II. Since there are still some uncertainties in determining from the pion photoproduction reaction the values of G_1 and G_2 of the $\gamma N\Delta$ vertex, we performed calculations for two sets of coupling constants. The dashed curves are calculated from using the highest value of G_1 = 2.68 (GeV^{-1}) and G_2 = −1.84 (GeV^{-2}) as determined by Jones and Scadron [26]. As for their application in $pp\gamma$ calculations these values are very close to the ones found in a recent analysis of Lee, who finds slightly higher values [39]: G_1 = 2.89 (GeV^{-1}) and G_2 = −2.18 (GeV^{-2}). The solid curves are from using the lowest value of G_1 = 2.0 (GeV^{-1}), G_2 = 0.0 (GeV^{-2}) as predicted by the vector dominance model. As a reference we also include the results (dotted curves) calculated from only the nucleonic contributions [Figs. 1(a) and 1(b)]. As can be seen in Fig. 8, the Δ excitation mechanisms increase the cross section in most of the range of kine-

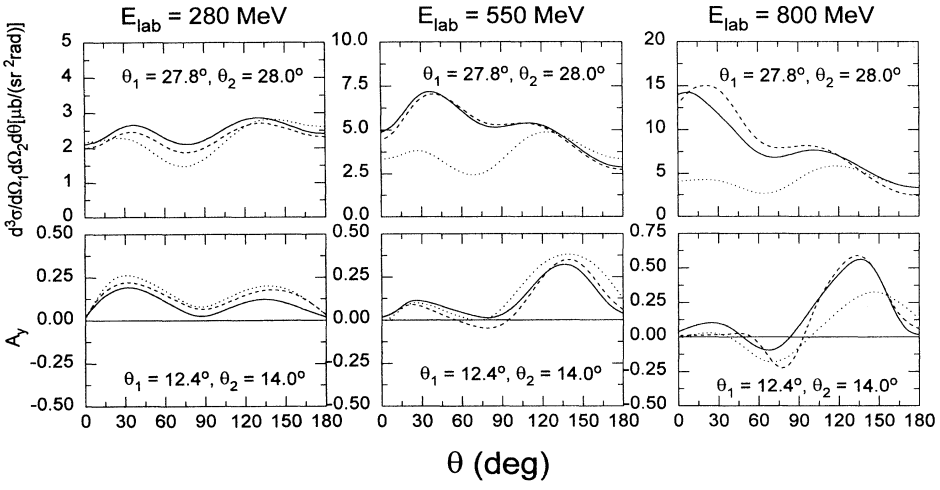

FIG. 7. The effect of the Δ rescattering diagrams on both the cross section and analyzing power in a coplanar geometry, at various laboratory energies. The solid line is the result including all diagrams, the dashed line is calculated with the nucleonic diagrams plus the single-scattering Δ-decay diagrams [Figs. 1(a)–1(c)] and the dotted line is calculated with only the nucleonic contributions [Figs. 1(a) and 1(b)]. In these calculations we took G_1 = 2.0 (GeV^{-1}) and G_2 = 0 (GeV^{-2}).

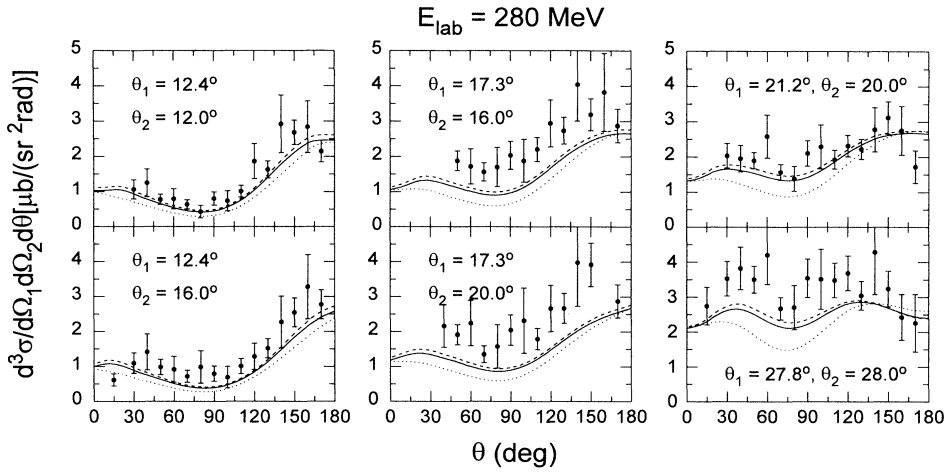

FIG. 8. Coplanar geometry $pp\gamma$ cross section in the laboratory frame as a function of the photon-emission angle at an incident energy of $E_{\rm lab} = 280$ MeV for various proton scattering angles θ_1 and θ_2. All diagrams were calculated using the NN and $N\Delta$ T matrices of Lee [11]. The dotted line corresponds to the calculation which only incorporates the nucleonic diagrams [Figs. 1(a) and 1(b)]. The results including Δ-decay diagrams are represented by the solid and the dashed lines. These correspond to the two choices of the $N\Delta\gamma$ coupling constants: the solid line stands for the results calculated with $G_1 = 2.0$ (GeV^{-1}) and $G_2 = 0$ (GeV^{-2}) and the dashed one for $G_1 = 2.68$ (GeV^{-1}) and $G_2 = -1.84$ (GeV^{-2}). The data [1] do *not* contain the arbitrary normalization factor of 2/3.

matics considered. The Δ-decay diagrams [Fig. 1(c)] are responsible for the largest part of the increase. However, the nucleonic contributions are still dominant at this low energy and the differences due to the use of two different sets of $\gamma N\Delta$ coupling constants are not particularly large. Nevertheless, the Δ effects clearly significantly bring the theoretical values closer to the data of the differential cross sections.

The Δ effects also improve the agreements with the data of the analyzing powers, as seen in Fig. 9. The agreement with the data is very good in most of the kinematic regions considered. Again, the differences between the results using two different sets of G_1 and G_2 are rather small. Clearly, it is necessary to consider the higher energy regions in order to have a critical test of our model of the Δ excitation and, in particular, to narrow down the values of G_1 and G_2 of the $\gamma N\Delta$ vertex.

To illustrate the increasing importance of the Δ mechanisms as energy increases, we show in Fig. 10 the inclusive photon production cross section as a function of photon energy at photon angle $\theta = 90°$ and $E_{\rm lab} = 280, 550$, and 800 MeV. At $E_{\rm lab} = 280$ MeV we find a general increase in the inclusive cross section, which has its maximum around photon energies of 90 MeV. At that point the increase is slightly more than the maximum increase we find in the results for the exclusive coplanar cross sections. At higher laboratory energies we clearly see the k dependence of the Δ-decay contributions, resulting in

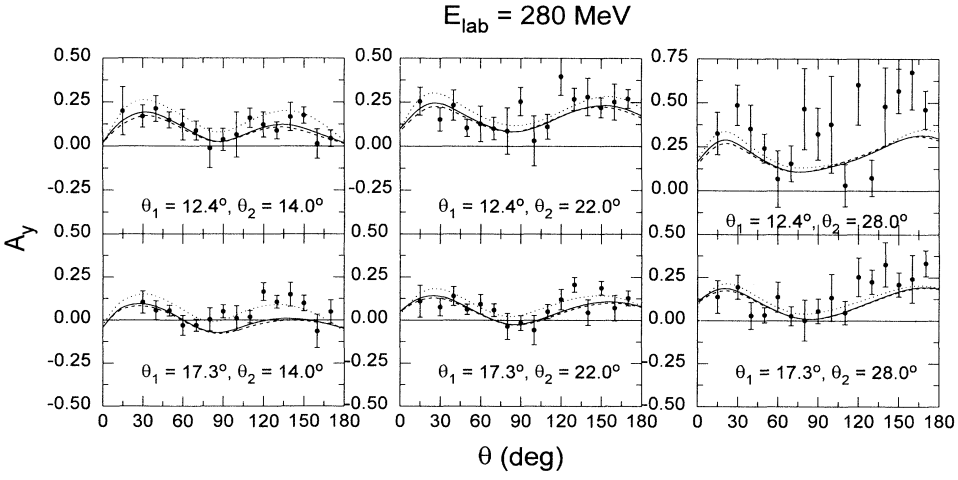

FIG. 9. Same as Fig. 8 for the analyzing power. The data are from Ref. [1] and have been multiplied by a factor of -1.

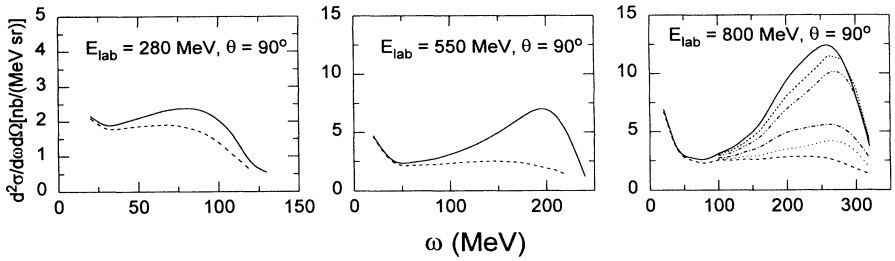

FIG. 10. Inclusive cross section at photon angle 90° at various laboratory energies as a function of photon momentum. The dashed line is the result with only the nucleonic contributions [Figs. 1(a) and 1(b)], the solid line is the full result including all diagrams calculated with $G_1 = 2.0$ (GeV^{-1}) and $G_2 = 0$ (GeV^{-2}). In the plot for $E_{\mathrm{lab}} = 800$ we also show the cumulative contributions of the partial waves: $J \leq 1$ (dotted), $J \leq 2$ (dash-dotted), $J \leq 3$ (dash-dot-dotted), and $J \leq 4$ (short dashed). The full result is calculated with $J \leq 9$.

peaks at the high end of the kinematically allowed photon energies. The cross section near the Δ peak is doubled by the Δ mechanisms at $E_{\mathrm{lab}} = 550$ MeV, and by a factor of about 5 at $E_{\mathrm{lab}} = 800$ MeV. The large enhancement of the Δ peak is mainly due to the resonant behavior of the Δ propagator, Eq. (22), and the dependence on the photon momentum of the vertex equations (15) and (18). This is in contrast to the results at $E_{\mathrm{lab}} = 280$ where the effect is due to strong interference of a small Δ contribution with the much larger nucleonic current contribution.

In the figure for $E_{\mathrm{lab}} = 800$ MeV we also plot the cumulative contributions of the partial waves for $J \leq 1$ to $J \leq 4$. The largest contributions are from the $J = 3$ partial wave ($^3F_3$). It is interesting to point out that the same large contribution from the $J = 3$ partial wave is also found in the study of $pp \to pn\pi^+$ reaction (Tables I and III of Ref. [40]). To have a unified description of both the pionic and electromagnetic excitation in pp scattering, it will be interesting to also have the $NN\gamma$ data at 800 MeV.

For future experimental tests of our model of the Δ excitation, we present our predictions of the exclusive cross sections and analyzing powers at $E_{\mathrm{lab}} = 550$ MeV (Fig. 11) and 800 MeV (Fig. 12). The calculations are identical to those of Figs. 8 and 9. The dotted curves are from calculations including only the nucleonic contributions. The solid and dashed curves are, respectively, calculated by using the $\gamma N\Delta$ coupling constants of vector dominance and Jones and Scadron [26]. As seen in both Figs. 11 and 12, including the Δ contributions drastically changes the differential cross sections. Hopefully, the forthcoming COSY experiment will have enough accuracy to distinguish the solid and dashed curves. This will help narrow down the values of G_1 and G_2 of the $\gamma N\Delta$ vertex, provided the other model-dependent parts of the present calculation, as discussed previously, are relatively small. Rather surprisingly, the inclusion of the Δ-decay diagrams has much less effect on the calculated analyzing powers. This suggests that the Δ-decay diagrams have at these energies and kinematics a similar spin structure (to the extent this is measured by the analyzing power) as the nucleonic contributions.

Finally, in regard to $pp\gamma$ experiments at high ener-

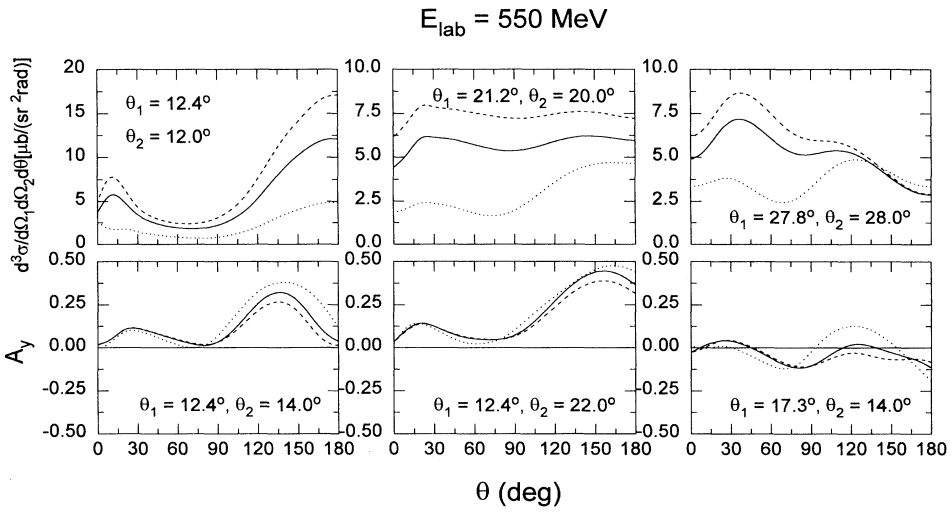

FIG. 11. Same as Figs. 8 and 9 but at an incident energy of $E_{\mathrm{lab}} = 550$ MeV.

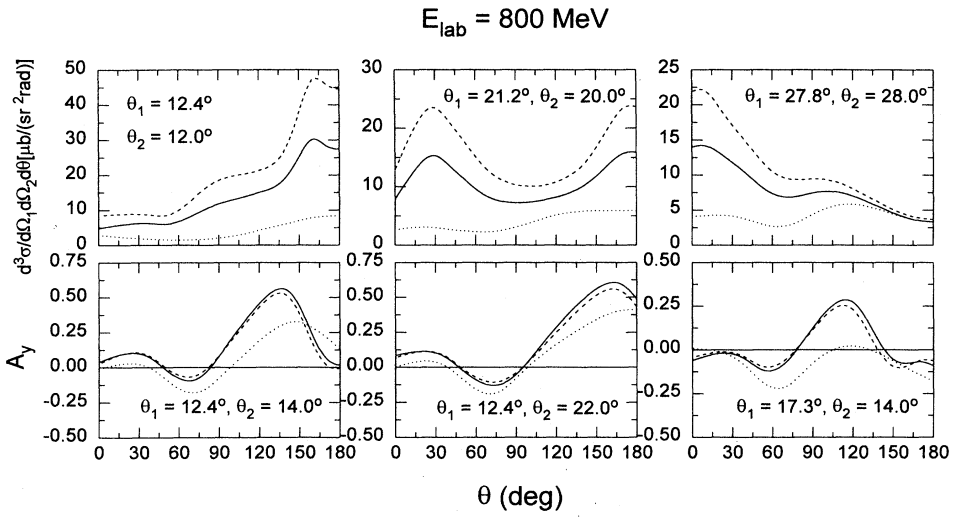

FIG. 12. Same as Figs. 8 and 9 but at an incident energy of $E_{\rm lab} = 800$ MeV.

gies we should mention the efforts of the authors of Ref. [41]. These authors performed a $pp\gamma$ experiment at $E_{\rm lab} = 730$ MeV. However, due to the experimental setup they probe a kinematical region which has relatively low photon energies. In the coplanar geometries for which we presented our calculations the photon energy in the initial NN c.m. frame ranges from 200 to 350 MeV. In the experiment of Ref. [41], the photon energy is below 150 MeV. The data from Ref. [41] show a rise at the high energy end of the kinematically reachable photon energies, possibly indicating an onset of the Δ effect. However, as can be seen from Fig. 10, the Δ effect reaches its maximum at much larger photon energies. Together with the large errors this makes the experiment less than optimal for studying the role of the Δ isobar in NN bremsstrahlung reactions. Also note that the effect of the Δ contributions found by the authors of Ref. [42] is not large enough to reconcile their calculation with the data.

IV. SUMMARY AND DISCUSSION

In this work we have developed an approach to investigate the pp bremsstralung at both low and intermediate energies. It is based on an extension of the coupled $NN \oplus N\Delta \oplus \pi NN$ model of Refs. [11, 12] to include the electromagnetic coupling with the N and Δ currents. The hadronic part of the model is consistent with NN scattering up to 1 GeV. The $\gamma N\Delta$ coupling is determined in the study of pion photoproduction in the P_{33} channel. The relativistic features of the one-baryon current matrix elements are treated exactly by performing the calculation directly in momentum space. In addition, the Δ rescattering contribution [Fig. 1(d)] is evaluated in this field.

We have shown that the Δ contribution can interfere strongly with the nucleonic contribution. As seen in Figs. 8 and 9, the Δ contribution can significantly improve the agreement with the data even at low energies below pion production threshold. Given the uncertainty in the normalization of the data, it remains to be seen if the remaining discrepancies with the data are due to these normalization problems or that higher-order interaction currents such as those due to the $\rho \to \pi\gamma$ and $\omega \to \pi\gamma$ couplings (decay diagrams) and $N\bar{N}\gamma$ (pair diagrams) can account for these discrepancies. A recent qualitative study which included decay diagrams in conjunction with the Δ effects (all in the Born approximation) found that these decay diagrams tended to reduce the effect of the Δ contributions [42]. It remains to be seen however, whether a calculation of these effects employing a full T matrix would substantiate these findings.

At intermediate energies, the Δ excitation dominates the $pp \to pp\gamma$ cross sections, as displayed in Figs. 10–12. Our predictions should be reasonable in guiding the experimental efforts. However, the employed coupled-channel model was constructed by fitting the NN phase shift data back in 1981 [43]. This has to be improved since the phase-shift data have been changed significantly recently [44]. Another important step is to extend the present approach to include the effective two-body current within the coupled-channel model. In particular, the $N\bar{N}\gamma$ couplings should be taken into account to fully restore the gauge-invariance condition of the model. However, a consistent inclusion of antiparticles in both the strong and electromagnetic interactions requires a reliable relativistic many-body theory. The present approach may also be extended for studying np bremsstralung at intermediate energies. This also requires the inclusion of (two-body) exchange currents within the coupled-channel model. Our effort in this direction will be published elsewhere.

ACKNOWLEDGMENTS

This work was supported in part by COSY, KFA-Juelich, Grant No. 41256714. One of the authors (F.d.J.) would like to thank the physics division of Argonne National Laboratory for the hospitality extended to him during two visits when part of this work was completed. This work was partially supported by the U.S. Department of Energy, Nuclear Physics Division, under Contract W-31-109-ENG-38.

[1] K. Michaelian *et al.*, Phys. Rev. D **41**, 2689 (1990).
[2] B.v. Przewoski, H.O. Meyer, H. Nann, P.V. Pancella, S.F. Pate, R.E. Pollock, T. Rinckel, M.A. Ross, and F. Sperisen, Phys. Rev. C **45**, 2001 (1991).
[3] R.L. Workman and H.W. Fearing, Phys. Rev. C **34**, 780 (1986); H.W. Fearing, Nucl. Phys. **A463**, 95c (1987).
[4] V. Herrmann and K. Nakayama, Phys. Rev. C **45**, 1450 (1992).
[5] V. Herrmann and K. Nakayama, Phys. Rev. C **46**, 2199 (1992).
[6] V.R. Brown, P.L. Anthony, and J. Franklin, Phys. Rev. C **44**, 2199 (1992).
[7] M. Jetter, H. Freitag, and H.V. von Geramb, Phys. Scr. **48**, 229 (1993).
[8] A. Katsogiannis and K. Amos, Phys. Rev. C **47**, 1376 (1993).
[9] J.A. Eden, D. Pluemper, M.F. Gari, and H. Hebach, Z. Phys. A **347**, 145 (1993).
[10] F. de Jong, K. Nakayama, V. Herrmann, and O. Scholten, Phys. Lett. B **333**, 1 (1994).
[11] T.-S.H. Lee, Phys. Rev. Lett. **50**, 1571 (1983); Phys. Rev. C **29**, 195 (1984).
[12] T.-S.H. Lee and A. Matsuyama, Phys. Rev. C **36**, 1459 (1987).
[13] G.E. Bohannon, L. Heller, and R.H. Thompson, Phys. Rev. C **16**, 284 (1977).
[14] L. Tiator, H.J. Weber, and D. Drechsel, Nucl. Phys. **A306**, 468 (1978).
[15] A. Szyjewicz and A.N. Kamal, in *Nucleon-Nucleon Interactions*, edited by F. Measday, H.W. Fearing, and A. Strathdee, AIP Conf. Proc. No. 41 (AIP, New York, 1978), p. 502; in *Few Body Systems and Nuclear Forces I*, edited by H. Zingl, M. Haftel, and H. Zankel, Springer Lecture Notes in Physics Vol. 82 (Springer, Berlin, 1978), p. 88.
[16] H. Nifenecker and J.A. Pinston, Annu. Rev. Nucl. Part. Sci. **40**, 113 (1990).
[17] V. Metag, Ann. Phys. **48**, 121 (1991).
[18] C. Naudet *et al.*, Phys. Rev. Lett. **62**, 2652 (1989).
[19] Gy. Wolf, W. Cassing, and U. Mosel, Nucl. Phys. **A552**, 549 (1993).
[20] H. Gacilazo and T. Mizutani, *πNN System* (World Scientific, Singapore, 1990).
[21] T.-S.H. Lee and A. Matsuyama, Phys. Rev. C **32**, 516 (1985).
[22] G.-H. Niephaus, M. Gari, and B. Sommer, Phys. Rev. C **20**, 1096 (1979).
[23] M. Lacombe *et al.*, Phys. Rev. C **21**, 861 (1980).
[24] S. Nozawa, B. Blankleider, and T.-S.H. Lee, Nucl. Phys. **A513**, 459 (1990).
[25] J.D. Bjorken and S.D. Drell, *Relativistic Quantum Files* (McGraw-Hill, New York, 1965).
[26] H.F. Jones and M.D. Scadron, Ann. Phys. **81**, 1 (1973).
[27] R. Davidson, N. Mukhopadhyay, and R. Wittman, Phys. Rev. Lett. **56**, 804 (1986).
[28] I. Blomqvist and J.M. Laget, Nucl. Phys. **A280**, 405 (1977).
[29] J.H. Koch, E.J. Moniz, and N. Ohtsuka, Ann. Phys. **154**, 99 (1984).
[30] B. ter Haar and R. Malfliet, Phys. Rep. **149**, 207 (1987).
[31] L.M. Nath and B.K. Battacharyya, Z. Phys. C **5**, 9 (1980).
[32] R.M. Davidson, Nimai C. Mukhopadhyay, and R.S. Wittman, Phys. Rev. D **43**, 71 (1991).
[33] H. Benmerrouche, R.M. Davidson, and N.M. Mukhopadhyay, Phys. Rev. C **38**, 2339 (1989).
[34] G.E. Brown and A.D. Jackson, *The Nucleon-Nucleon Interaction* (North-Holland, Amsterdam, 1976).
[35] L. Heller, S. Kumano. J.C. Martinez, and E.J. Moniz, Phys. Rev. C **35**, 718 (1987).
[36] K. Nakayama, S. Krewald, and J. Speth, Nucl. Phys. **A451**, 243 (1986).
[37] V. Herrmann, K. Nakayama, O. Scholten, and H. Arellano, Nucl. Phys. **A582**, 568 (1995).
[38] V. Herrmann and K. Nakayama, Phys. Lett. B **333**, 251 (1990).
[39] T.-S.H. Lee (unpublished).
[40] A. Matsuyama and T.-S.H. Lee, Phys. Rev. C **34**, 1900 (1986).
[41] B.M.K. Nefkens, O.R. Sander, and D.I. Sober, Phys. Rev. Lett. **38**, 876 (1977).
[42] M. Jetter and H.W. Fearing, Triumf Report No. TRI-PP-94-90.
[43] R.A. Arndt and L.D. Roper, Phys. Rev. D **25**, 2011 (1982).
[44] SAID Interactive Dial-In System, R.A. Arndt, private communication.